A Correlated Noise Calibration Standard for Interferometric, Polarimetric, and Autocorrelation Microwave Radiometers

Christopher S. Ruf, *Fellow, IEEE,* and Jikang Li

***Abstract*—A new type of calibration standard is presented which produces a pair of microwave noise signals to aid in the characterization and calibration of correlating radiometers. The Correlated Noise Calibration Standard (CNCS) is able to generate pairs of broad bandwidth stochastic noise signals with a wide variety of statistical properties. The CNCS can be used with synthetic aperture interferometers to generate specific visibility functions. It can be used with fully polarimetric radiometers to generate specific third and fourth Stokes parameters of brightness temperature. It can be used with spectrometers to generate specific power spectra and autocorrelations. It is also possible to combine these features and, for example, to generate the pair of signals that would be measured by a fully polarimetric, spectrally resolving, synthetic aperture radiometer at a particular pair of polarizations and antenna baselines for a specified scene over a specified frequency band. Algorithms are presented to construct signals with the desired statistical properties. Also presented is a description of the key hardware design challenges that were associated with fabrication of the first unit. CNCS performance is demonstrated by characterization tests of a pair of microwave interferometer radiometer receivers.**

***Index Terms*—Calibration, random noise, radiometers, polarimetry.**

I. Introduction

THREE TYPES OF microwave radiometers measure the partial correlation between a pair of random Gaussian signals. Spatial interferometers cross correlate signals originating from two separated antennas to sample Fourier components of the angular brightness temperature distribution. This was first attempted for radio astronomy imagers [10], [28] and later for earth remote sensing [9], [19]. Temporal autocorrelators correlate a single signal with a time delayed version of itself to resolve its frequency spectrum. This was also first attempted by radio astronomy spectrometers [8] and later adopted for incoherent scatter ionospheric radars [5], [18] and earth remote sensing [4], [20]. It is also possible to combine these two techniques and obtain both a spatially and spectrally resolved image of the incident radiation and this has been done successfully by radio astronomers [15]. The third type of correlating radiometer measures the full Stokes parameters of the radiation by cross correlating signals originating from orthogonal linear components of polarization. Again, radio astronomers have successfully developed such instruments [3], and its application to earth remote sensing in combination with spatial interferometry is under study [14]. There has been considerable interest recently in development of polarimetric correlating radiometers for earth remote sensing in which the orthogonally polarized signals originate from a single antenna aperture. The application is detection of a modulation in the brightness temperature of the ocean surface caused by wind direction [29], [30], and several such sensors have been built [16], [23]. To date, no sensor has been built which incorporates all three types of correlators simultaneously—to spatially and spectrally resolve each of the four Stokes parameters—but this is in principle also possible.

Traditional noncorrelating radiometers measure the total microwave noise power present in the receiver by integrating the square of the signal originating from a single antenna at a single polarization. This is technically also a type of correlating radiometer—measuring the self-correlation—and has been implemented as such using correlator-based hardware [6]. However, the vast majority of self-correlating (often referred to as total power) radiometers use an analog square law detector diode instead [27]. Total power radiometers are traditionally tested and calibrated using calibration standards that provide two or more known brightness temperatures. The standards must generate microwave noise with a known and stable degree of self-correlation. Since any signal is fully correlated with itself, the problem reduces to generation of a single stable source of noise power. This requirement can be met using a black body source having the property that its brightness temperature is equal to its physical temperature. The design requirements for such a calibration standard reduce to providing a known and stable thermal environment for the black body load. The development, testing and calibration of total power radiometers have been enormously simplified by the ready availability of this established brightness temperature standard.

Correlating radiometers should similarly benefit from a suitable calibration standard. In fact, the need for extremely accurate calibration is in this case arguably more pressing because of the added complexity of the hardware and the much smaller partially correlated noise powers that are typically measured [21], [26]. A suitable standard should be able to generate two signals with a known and stable level of partial correlation. No device as simple as a black body load can provide this. Numerous approaches have been taken to calibrating correlation radiometers. Brightness temperature images produced by the spatial interferometer ESTAR have been calibrated and validated using model

Manuscript received September 16, 2002; revised June 16, 2003. This work was supported in part by the National Aeronautics and Space Administration under Grants NAG5-8005, NAG5-9967, and NAG5-9762.

The authors are with the Department of Atmospheric, Oceanic and Space Sciences, University of Michigan, Ann Arbor, MI 48109 USA (e-mail: cruf@umich.edu).

Digital Object Identifier 10.1109/TGRS.2003.815971

predictions of the expected scene [12], [24]. This is a valuable end-to-end test of sensor performance because it includes all potential sources of error. However, it is limited in its accuracy by the quality of the predictive model that is used and it cannot be easily adapted as a diagnostic tool during sensor development in the laboratory. In an effort to address these limitations, a modification to the traditional black body load has been developed that is capable of producing important subsets of the range of partial correlations possible between two microwave noise signals [7]. This polarized load consists of two traditional black body absorbers maintained at different physical temperatures. The microwave noise power emitted by them is combined quasi-optically with a polarizing grid. The relative alignment between the polarizing grid and the polarization reference axes of a radiometer's antenna determine what Stokes parameters a polarimetric radiometer will measure. Variations in the relative alignment provide a set of calibration references against which to verify sensor performance in a manner roughly analogous to total power radiometer calibration. This is a very useful tool for sensor development that has been adopted by other research groups [11]. It, too, has some limitations. The device was developed specifically for use with polarimetric radiometers and cannot be easily adapted to more general use by the other two types of correlating radiometers. Two practical issues with the design of a polarized load are also noteworthy. Very precise mechanical alignment is required to guarantee known and stable Stokes parameters. And the requirement that two large black body loads be in close proximity but at significantly different physical temperatures that are well known and stable can make the temperature control problem challenging. For all of these reasons, we consider here an alternative method for generating partially correlated noise sources to serve as a calibration standard for all three types of correlation radiometers.

II. Description of the CNCS

A. Overview

The heart of the correlated noise calibration standard (CNCS) is a commercial dual-channel arbitrary waveform generator (AWG) [13]. In our case, we use a Tektronix Model AWG2020 with a 250-MHz clock speed and 2 Msamples of memory but other brands and models are also suitable. Such AWGs typically consist of a pair of high resolution digital to analog converters (DACs) that are synchronously triggered by a common high speed clock. The digital inputs to the DACs are stored as a pair of "lookup tables" (LUTs) in memory. Values are preloaded into the LUTs, either from an internal library of standard functions or via a communication link to an external control computer. The output clock is then activated and the values in the LUTs are routed to the DACs. It is common to cycle the pointer to the LUT back to the beginning after it reaches the end. In this manner, the output from a DAC is inherently periodic. Its period is set by the length of the LUT (i.e., the available memory in the AWG) together with the clock rate. The clock rate also determines the maximum possible bandwidth of the output signal.

Use of an AWG permits a very significant amount of freedom in choosing the output analog wave forms. If the LUT is preloaded from a control computer with random numbers generated in a high-level software language, then the analog output signal can have a wide variety of specific statistical properties. For example, it is possible to control the noise bandwidth and variance of individual signals, which is of use for calibrating self-correlating radiometers. It is possible to finely control the spectral shape of the noise (its color), which is of use for calibrating autocorrelation radiometers. It is possible to independently control both quadrature components of partial correlation (i.e., the complex correlation) between two signals, which is of use for calibrating either interferometric or polarimetric radiometers. And it is possible to vary the complex partial correlation between signals as a function of frequency, which would be of use for calibration of a hypothetical radiometer that performed all three types of correlations simultaneously.

The remainder of this section summarizes the underlying statistical properties of the random variables that are used to generate the values in the LUTs. In the following sections, those properties are then related to the brightness temperature, visibility function, Stokes parameters, and brightness temperature spectra measured by correlating microwave radiometers. In Section IV, specific algorithms are described that are used to generate the values loaded into the LUTs to produce the desired noise statistics. Limitations on the accuracy and precision of the desired statistics (primarily resulting from clock speed and LUT memory constraints) are also discussed where appropriate. Section V presents first experimental results using the CNCS to characterize a correlation radiometer system under development to image precipitation.

B. Box–Müller Transformation and Gaussian Covariance

The starting point for generation of random numbers in many high-level software languages is the uniformly distributed random number between zero and one. A Gaussian distributed random number g with zero mean and unity variance can be constructed from a pair of such independent uniformly distributed numbers u_1 and u_2 by use of the Box–Müller transformation [2]

$$g = \sqrt{-2\log(u_1)}\cos(u_2\pi). \tag{1}$$

A sequence of P Gaussian distributed random numbers $x_1, \ldots, x_P$ with zero mean, standard deviations $\sigma_1, \ldots, \sigma_P$, and cross correlations r_{ij} for $i, j = 1, \ldots, P$ can be constructed from a sequence of P independent Gaussian numbers $g_1, \ldots, g_P$ by the following set of linear transformations

$$x_i = \left(\sum_{k=1}^{i} \gamma_{ik} g_k\right) \sigma_i \tag{2a}$$

where

$$\gamma_{i1} = r_{i1}, \qquad \text{for } i = 1, \ldots, P \tag{2b}$$

$$\gamma_{ii} = \sqrt{1 - \sum_{k=1}^{i-1} \gamma_{ik}^2}, \qquad \text{for } i = 2, \ldots, P \tag{2c}$$

$$\gamma_{ij} = \frac{r_{ij} - \sum_{k=1}^{j-1} \gamma_{jk}\gamma_{ik}}{\gamma_{jj}}, \quad \text{for } i = 3, \ldots, P,\ j = 1, \ldots, i-1. \tag{2d}$$

A Gaussian vector constructed in this manner will have the desired correlation statistics, namely

$$\langle x_i \rangle = 0, \qquad \text{for } i = 1, \ldots, P \tag{3a}$$

and

$$\langle x_i x_j \rangle = r_{ij}\sigma_i\sigma_j, \qquad \text{for } i, j = 1, \ldots, P \tag{3b}$$

where $-1 \leq r_{ij} \leq 1$ in general and $r_{ii} = 1$ for the case of self-correlation.

Equations (1) and (2) are used to construct real-valued Gaussian distributed random vectors. The algorithm can be adapted to construct complex Gaussian distributed variables as well. Define the two complex Gaussian random numbers c_A and c_B as

$$c_A = x_1 + jx_2 \tag{4a}$$

$$c_B = x_3 + jx_4 \tag{4b}$$

where $x_1, \ldots, x_4$ are four partially correlated Gaussian random numbers. The complex correlation, r_c, between c_A and c_B is defined as

$$r_{AB} = r_R + jr_I = \rho e^{j\theta} \equiv \frac{\langle c_A c_B^* \rangle}{\sigma_A \sigma_B} \tag{5}$$

where σ_A and σ_B are the standard deviations of the two complex numbers, given by

$$\sigma_n \equiv \sqrt{\langle c_n c_n^* \rangle}, \qquad \text{for } n = A, B. \tag{6}$$

Note that r_{AB} in (5) is commonly referred to as the normalized coherence in radio astronomy. Inserting (4) into (5) and collecting real and imaginary components gives

$$\frac{\langle x_1 x_3 \rangle}{\sigma_A \sigma_B} = \frac{\langle x_2 x_4 \rangle}{\sigma_A \sigma_B} = \frac{\rho \cos\theta}{2} \tag{7a}$$

$$-\frac{\langle x_1 x_4 \rangle}{\sigma_A \sigma_B} = \frac{\langle x_2 x_3 \rangle}{\sigma_A \sigma_B} = \frac{\rho \sin\theta}{2} \tag{7b}$$

where ρ is the magnitude and θ the phase of the complex correlation coefficient. Equation (7) can be used to specify the required correlation statistics needed to construct c_A and c_B from four independent Gaussian random variables $g_1, \ldots, g_4$ using the same procedure developed for real-valued Gaussian vectors. Specifically, define the partial correlation matrix R between the four real-valued elements $x_1, \ldots, x_4$ of a Gaussian vector as

$$R = \begin{bmatrix} 1 & 0 & \frac{\rho\cos\theta}{2} & -\frac{\rho\sin\theta}{2} \\ 0 & 1 & \frac{\rho\sin\theta}{2} & \frac{\rho\cos\theta}{2} \\ \frac{\rho\cos\theta}{2} & \frac{\rho\sin\theta}{2} & 1 & 0 \\ -\frac{\rho\sin\theta}{2} & \frac{\rho\cos\theta}{2} & 0 & 1 \end{bmatrix}. \tag{8}$$

If c_A and c_B are constructed from $x_1, \ldots, x_4$ using (2) (with $P = 4$), (4), and (8), then they will have the desired complex statistical properties.

C. Sampling and Bandwidth Considerations

Assume the LUT in the AWG contains $2N + 1$ entries. Let each entry correspond to a discrete time sample a_n, $n = -N, -N+1, \ldots, N$, of a function $a(t)$ at time $t_n = nT_s$, where T_s is the sampling interval. The output signal $b(t)$ produced by the AWG can be represented as a sequence of discrete pulses, weighted by a_n, that has been passed through an ideal (rectangular) lowpass filter with a cut-off frequency at $f_s/2$, where $f_s = 1/T_s$. The output signal can be written as

$$b(t) = \sum_{n=-N}^{N} a_n \operatorname{sinc}\left(\pi \frac{t - nT_s}{T_s}\right), \quad \text{for} -\left(N + \frac{1}{2}\right)T_S \leq t < \left(N + \frac{1}{2}\right)T_S \tag{9}$$

where $\operatorname{sinc}(x) = \sin(x)/x$. The Nyquist sampling theorem guarantees that the output signal $b(t)$ will be equal to the original signal $a(t)$, provided $a(t)$ is also assumed to be bandlimited with highest frequency component less than $f_s/2$. This statement must be qualified by the fact that $b(t)$ is defined only over the interval $[-(N+1/2)T_s, (N+1/2)T_s)$ whereas $a(t)$ must be defined for all time to be truly bandlimited. The time window imposed on $b(t)$ is equivalent to a convolution of $\operatorname{sinc}[\pi(2N+1)T_s f]$ with $A(f)$, the Fourier transform of $a(t)$. The convolution essentially acts as a running average of $A(f)$ over a bandwidth $1/(2N+1)T_s$. In other words, any spectral variations present in $A(f)$ on scales finer than $1/(2N+1)T_s$ will be washed out in $B(f)$, the Fourier transform of $b(t)$.

In practice, the pointer to the LUT cycles repeatedly through its entries, making the output signal from the AWG periodic with period $T_p = (2N+1)T_s$. Define $c(t)$ as that periodic signal. It is composed of an infinite concatenation of replicas of $b(t)$ every T_p seconds and can be written as

$$c(t) = \sum_{n=-\infty}^{\infty} b(t - nT_p) = b(t) \otimes \sum_{n=-\infty}^{\infty} \delta(t - nT_p) \tag{10}$$

where $\otimes$ denotes convolution, and $\delta(t)$ is the Dirac delta function. The Fourier transform of $c(t)$ is given by

$$C(f) = f_p \sum_{n=-\infty}^{\infty} B(nf_p)\delta(f - nf_p) \tag{11}$$

where $f_p = 1/T_p$ is the frequency of periodicity of the output signal. Thus, the spectrum of the output signal consists of a series of discrete frequency components spaced every f_p Hz and weighted by the spectrum $B(f)$.

In terms of the particular AWG used in our design, the sample rate is $f_s = 250$ MHz, and the available memory for the LUT is $2N + 1 = 10^6$ samples for each of its two output signals. The sample rate implies that a maximum signal bandwidth of 125 MHz can be generated. The periodicity of the output signal is $f_p = f_s/(2N+1) = 250$ Hz. The periodicity implies that an

output signal can be generated with spectral variations defined every 250 Hz.

III. Relationship Between Brightness Temperature and Random Numbers

In the case of total power radiometers, a measurement is made of the expectation of the square of the voltage incident on the detector. The voltage is modeled as a zero-mean wide-sense stationary Gaussian random process. Let x be that voltage. It is related to the brightness temperature T_B by [27]

$$\langle x^2 \rangle = G(T_B + T_{\rm Rx}) \tag{12}$$

where G is the radiometer's system gain and $T_{\rm Rx}$ is the receiver noise temperature. Small additional biases in the measurements (due, for example, to detector and digitizer voltage offsets) are not considered here. Calibration of a total power radiometer typically consists of measuring $\langle x^2 \rangle$ for two known values of T_B to determine G and $T_{\rm Rx}$. In the case of correlating radiometers, the self-correlation of individual channels (be they individual antennas in an interferometric array or individual polarizations in a fully polarimetric radiometer) will likewise produce a measurement that is linearly proportional to the system noise temperature $T_{\rm sys} = T_B + T_{\rm Rx}$ of that channel. In other words, the variance of individual channels is independently determined by their system noise.

The partial correlation between channels of a polarimetric correlating radiometer is related to the Stokes parameters of the brightness temperature [1]. Let x_V and x_H represent the voltages originating from the vertically and horizontally polarized output ports of a single antenna. Their complex correlation is related to the incident brightness by

$$\sigma_V^2 \equiv \langle x_V x_V^* \rangle = G_V(T_{B,V} + T_{Rx,V}) \tag{13a}$$

$$\sigma_H^2 \equiv \langle x_H x_H^* \rangle = G_H(T_{B,H} + T_{Rx,H}) \tag{13b}$$

$$r_{VH}\sigma_V\sigma_H \equiv \langle x_V x_H^* \rangle = G_{VH}(T_3 + jT_4) \tag{13c}$$

where G_V, G_H, and G_{VH} are the gains of each signal path, $T_{B,V}$ and $T_{B,H}$ are the vertically and horizontally polarized brightness temperatures, T_3 and T_4 are the third and fourth Stokes parameters, r_{VH} is the complex partial correlation between x_V and x_H, $T_{Rx,V}$ and $T_{Rx,H}$ are the noise temperatures of the vertically and horizontally polarized receivers. The terms $T_{Rx,V}$ and $T_{Rx,H}$ do not appear in (13c) because these two noise sources originate from different receivers and are therefore uncorrelated.

The partial correlation between channels of an interferometric correlating radiometer is related to the real and imaginary components of the visibility of the angular brightness temperature distribution $V = V_R + jV_I$. [10], [19]. Let x_i and x_j represent the voltages originating from the ith and jth channels of an interferometer array. Their complex correlation is related to the incident brightness by

$$\sigma_{ii}^2 \equiv \langle x_i x_i^* \rangle = G_{ii}(T_{B,i} + T_{Rx,i}) \tag{14a}$$

$$\sigma_{jj}^2 \equiv \langle x_j x_j^* \rangle = G_{jj}(T_{B,j} + T_{Rx,j}) \tag{14b}$$

$$r_{ij}\sigma_i\sigma_j \equiv \langle x_i x_j^* \rangle = G_{ij}(V_R + jV_I) \tag{14c}$$

where G_{ii}, G_{jj}, and G_{ij} are the gains of each signal path; $T_{B,i}$ and $T_{B,j}$ are the brightness temperatures integrated over the entire antenna pattern of the individual array elements; r_{ij} is the complex partial correlation between x_i and x_j; and $T_{Rx,i}$ and $T_{Rx,j}$ are the noise temperatures of the two receivers. The terms $T_{Rx,i}$ and $T_{Rx,j}$ do not appear in (14c) because these two noise sources originate from different, receivers and are therefore uncorrelated.

The partial correlation between a signal and a time delayed version of itself by an autocorrelation radiometer is related to the inverse Fourier transform of the brightness temperature spectrum, $T_B(f)$, according to the Weiner–Khinchin theorem [17]. Let x_t and $x_{t+\tau}$ represent samples at times t and $t+\tau$ of the voltage to be autocorrelated. Their complex correlation is related to the brightness temperature spectrum by

$$\sigma_x^2 \equiv \langle x_t x_t^* \rangle = G(T_B + T_{\rm Rx}) \tag{15a}$$

$$r_{t+\tau,t}\sigma_x^2 \equiv \langle x_{t+\tau} x_t^* \rangle = GF^{-1}\{T_B(f)\} \tag{15b}$$

where G is the system gain, T_B is the integrated brightness temperature across the passband of interest; $T_{\rm Rx}$ is the receiver noise temperature, F^{-1} denotes the inverse Fourier transform; and it is recognized that the variance of x is the same at times t and $t+\tau$, since x is wide sense stationary. It is more customary to express (15b) as the autocorrelation of x, $R_x(\tau) = \langle x_{t+\tau} x_t^* \rangle$, but we use the partial correlation notation to be consistent with the earlier expressions.

IV. Construction of AWG Lookup Tables

A. Bandwidth and $\sin c$ Interpolation

If each element of the AWGs LUT is an independent sample of a Gaussian random variable, then the highest frequency component of the power spectrum of the noise generated at the output will be $f_s/2$. One simple way to reduce the noise bandwidth is to reduce the sample rate, f_s, while using the same LUT. However, it is useful to maintain a consistent maximum sample rate while still being able to modify the bandwidth. If different LUT files with different bandwidths all have the same sample rate, then they can be easily combined together to create more complex noise spectra by superposition. There are also a number of other useful ways in which the noise statistics can be altered. It is convenient to maintain a consistent sample rate in all of these cases so that any of the resulting LUT files can be combined together by simple linear combinations of the individual LUT elements. For the case of reducing the bandwidth, the effect of a reduced sample rate can be duplicated at the maximum rate by placing independent samples at evenly spaced intervals in the LUT and then filling in the remaining elements using $\sin c$ interpolation between the independent samples. $\sin c$ interpolation is used because it has the property that no additional frequency components are added to the signal by the interpolation, thus guaranteeing the same noise bandwidth as that with the reduced sample rate. Specifically, assume independent noise realizations are placed every Mth element in the LUT, at $a_{-N}, a_{-N+M}, a_{-N+2M}, \ldots, a_N$. Define an intermediate element a_k by

$$a_k = \sum_{n=-2N,-2N+M,-2N+2M,\ldots}^{2N} a_n \sin c\left(\pi \frac{k-n}{M}\right), \quad \text{for } k = -N+1, -N+2, \ldots, N-1 \tag{16}$$

where it is recognized that $a_n = a_{n+2N+1}$ due to the periodic nature of the output signal. Thus, each intermediate element a_k is a weighted average of all the independent elements, $a_{-N}, a_{-N+M}, a_{-N+2M}, \ldots$, with the weighting determined by the value of the $\sin c$ function. In principle, the summation in (16) should extend to $\pm\infty$, but it is in practice truncated as noted due to the rapid decay of the $\sin c$ function for large arguments. With all $2N+1$ elements of the LUT filled in this manner and the output sampled at f_s, the output signal power spectrum will extend only over $\pm f_s/2M$.

B. Baseband-to-IF Software Modulation

The power spectrum of a signal generated using $\sin c$ interpolation is centered at dc (0 Hz). It is useful to be able to generate noise power spectra with a variable bandwidth and center frequency. The bandwidth of such a signal can be adjusted using $\sin c$ interpolation. The center frequency of the power spectrum can then be moved away from dc by amplitude modulation. If the maximum frequency component of the power spectrum after modulation is below the AWG limit of $f_s/2$, then the modulation can be performed in software after generating the noise realizations and prior to transferring the samples to the LUT. Specifically, assume a set of baseband samples, $a_{-N}, a_{-N+1}, \ldots, a_N$, have been prepared which would have produced a power spectrum centered at dc and with bandwidth f_s/M. Define the in phase modulated samples a_n^I by

$$a_n^I = a_n \cos(2\pi f_m n T_s), \qquad \text{for } n = -N, -N+1, \ldots, N \tag{17a}$$

where f_m is the desired center frequency. The noise produced by loading a_n^I into the LUT will have a power spectrum extending over $f_m \pm f_s/2M$ (provided the highest frequency component $(f_m + f_s/2M)$ is less than the maximum allowable frequency of $f_s/2$). Quadrature phase modulated samples a_n^Q can be similarly defined by

$$a_n^Q = a_n \sin(2\pi f_m n T_s), \qquad \text{for } n = -N, -N+1, \ldots, N. \tag{17b}$$

Both types of modulation will produce output signals with similar power spectra. However, the orthogonality of the sine and cosine carrier signals forces them to be uncorrelated. These signals can be combined in software as the real and imaginary components of a complex signal. Specifically, two signals having a complex partial correlation with arbitrary phase and magnitude can be generated by the following procedure: 1) define four uncorrelated, unity variance Gaussian random processes with samples at $n = -N, -N+1, \ldots, N$ as

$$[g_1]_n = \frac{a_n^I}{\langle a_n^I a_n^I \rangle^{1/2}} \tag{18a}$$

$$[g_2]_n = \frac{a_n^Q}{\langle a_n^Q a_n^Q \rangle^{1/2}} \tag{18b}$$

$$[g_3]_n = \frac{b_n^I}{\langle b_n^I b_n^I \rangle^{1/2}} \tag{18c}$$

$$[g_4]_n = \frac{b_n^Q}{\langle b_n^Q b_n^Q \rangle^{1/2}} \tag{18d}$$

where a_n and b_n are two independent random processes with power spectra centered at dc and bandwidths sufficiently narrow to permit software modulation; 2) samples of the four partially correlated random variables, $x_i\, i = 1, \ldots, 4$, are generated from the g_i in (18) by using (2) and (8) for particular values of θ and ρ. These values are the desired phase and magnitude, respectively, of the complex partial correlation between the two complex random variables; 3) samples of the two complex random variables are generated by

$$[c_A]_n = [x_1]_n + [x_2]_n \tag{19a}$$

$$[c_B]_n = [x_3]_n + [x_4]_n. \tag{19b}$$

By this procedure, the output signals, $c_A(t)$ and $c_B(t)$, generated by the AWG will have the desired complex partial correlations as described by (5).

C. IF-to-RF Hardware Modulation

In practice, noise power spectra are often desired at frequencies much higher than the maximum of $f_s/2$ available at the output of the AWG. In this case, the AWGs IF signals (after quadrature software modulation) can be upconverted with an external hardware modulator to the desired RF frequency range. A block diagram of the modulator used for the CNCS is shown in Fig. 1. In order to maintain coherence between the two signals, upconversion must be performed with a common local oscillator (LO). The LO distribution network then presents a potential signal path for unwanted crosstalk between the two arms of the modulator. Because of this, two details of the modulator design are critical to maintaining the desired partial correlation between signals. Crosstalk between the two arms of the modulator must be kept extremely low. Blockage of leakage at RF frequencies is accomplished by the liberal use of isolators. Blockage of leakage at IF frequencies is accomplished by employing sharp highpass filters (coax-to-waveguide-to-coax transitions) in the LO distribution network (see Fig. 1 for details). These highpass filters provide superior blocking of the IF signals which are, in practice, the dominant source of leakage between channels of the CNCS. Leakage of the LO signal itself into the two RF signal lines can also introduce unwanted correlation. This is minimized by the use of second harmonic upconversion mixers with high LO-to-RF isolation. Active cold loads—consisting of LNAs installed backward followed by isolators for improved impedance match—provide a low background brightness temperature on which to add the correlated noise signals via directional couplers.

D. Prewhitening Noise Color

In practice, a number of nonideal characteristics of the CNCS hardware contribute to a "coloring" of the actual noise spectrum that is produced. The noise is considered colored if its power spectral density is not uniform across its entire passband. It can be corrected by intentionally coloring, or "prewhitening" the AWG signal with the inverse of the measured nonuniformity. This is implemented by breaking a wideband signal up into a number of much narrower frequency bands. In our case, for example, an RF noise signal covering a passband from 10.685–10.715 GHz is constructed by summing 30 separate signals, each with 1-MHz bandwidth and centered in 1-MHz frequency increments across the passband. Construction of each of the noise components uses the baseband-to-IF software

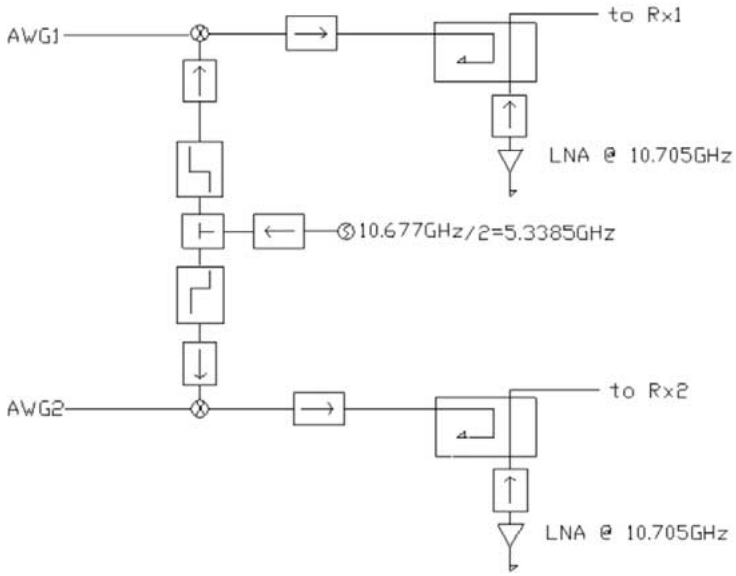

Fig. 1. Block diagram of upconversion modulator used by the CNCS to move the lower frequency signal pair generated by the AWG up to a useful RF frequency. Liberal use is made of isolators to reduce crosstalk between the two AWG signals at RF frequencies. Highpass filters in the LO distribution network reduce lower frequency leakage. A second harmonic upconversion mixer helps to reduce LO leakage into the signal paths. Active cold loads—using LNAs installed backward—provide a low background brightness temperature on which to add the correlated noise signals.

modulation technique described above to generate 30 independent IF subbands with 1-MHz bandwidth between 26 and 56 MHz. The AWG output signal is the sum of all 30 subbands. The AWG output is then upconverted to a center frequency of 10.700 GHz by the IF-to-RF modulator. Initially, each of the 1-MHz components has equal amplitude. Measurements are then made of the resulting RF spectrum, including any coloration introduced by the AWG or modulator. The amplitudes of each 1-MHz component are then individually adjusted, or prewhitened, so that the final RF spectrum is flat.

V. Laboratory Demonstration

A. CNCS Noise Power Spectrum

Screen shots of a spectrum analyzer showing the noise power spectrum produced by the CNCS are shown in Fig. 2(a)–(c). Fig. 2(a) shows the spectrum that is produced by the AWG when statistically independent Gaussian noise realizations are loaded into each element of its LUT. This is the widest bandwidth noise spectrum possible for the AWG to produce. Since the original noise realizations are spectrally flat, it also includes all coloration introduced by the hardware. In particular, note that the spectrum rolls off above $\sim$ 100 MHz due to lowpass characteristics of the signal output stage of the AWG. Fig. 2(b) shows a spectrum that has been band limited to 30 MHz and upconverted to a center frequency of 41 MHz using the $\sin c$ interpolation and baseband-to-IF software modulation techniques described above. Note that there is still some coloration present. Fig. 2(c) shows a spectrum with the same 30-MHz passband but with prewhitening applied to reduce much of the colored spectral features evident in Fig. 2(b).

B. Calibration of Radiometer Measurements

The CNCS has been tested using digitizing correlation radiometers that are part of the technology development effort associated with the Global Precipitation Measurement mission [22]. The radiometers operate at 10.7 GHz with a bandwidth of approximately 30 MHz. RF input signals are downconverted by the radiometers to an IF passband centered at 41 MHz and are then digitized at 125 Msamples/s. Digitized signals from a pair of the receivers are transferred to a field programmable gate array chip where they are self- and cross-correlated with two-bit precision. The RF test signals fed into the receivers from the CNCS are centered at 10.7 GHz with a bandwidth of 60 MHz and were prewhitened for spectral flatness.

The test signals from the CNCS include a (desired) component originating at the AWG and other noise components arising from thermal emission by the modulator hardware and interconnecting cabling. These other components would in general be statistically independent between the two signal paths. There is also the possibility of an additional correlated component of the signal beyond that generated by the AWG due to leakage and crosstalk in the modulator. The signals entering the two receivers can be written as

$$x_A = G_A c_A + d_A + e \tag{20a}$$

$$x_B = G_B c_B + d_B + e \tag{20b}$$

where $G_{A,B}$ are the gains of the two receivers, $c_{A,B}$ are the two signals generated by the AWG and given by (19), $d_{A,B}$ are uncorrelated signals due to independent thermal emission by the hardware in the two signal paths, and e is an additional signal that is common to the paths. The self-correlation of each individual signal and the real component of the complex cross correlation of the pair of signals produce raw measurements given by

$$\langle x_A^2 \rangle = G_A^2 \langle c_A^2 \rangle + \langle d_A^2 \rangle + \langle e^2 \rangle \tag{21a}$$

$$\langle x_B^2 \rangle = G_B^2 \langle c_B^2 \rangle + \langle d_B^2 \rangle + \langle e^2 \rangle \tag{21b}$$

$$\langle x_A x_B \rangle = G_A G_B \langle c_A c_B \rangle + \langle e^2 \rangle. \tag{21c}$$

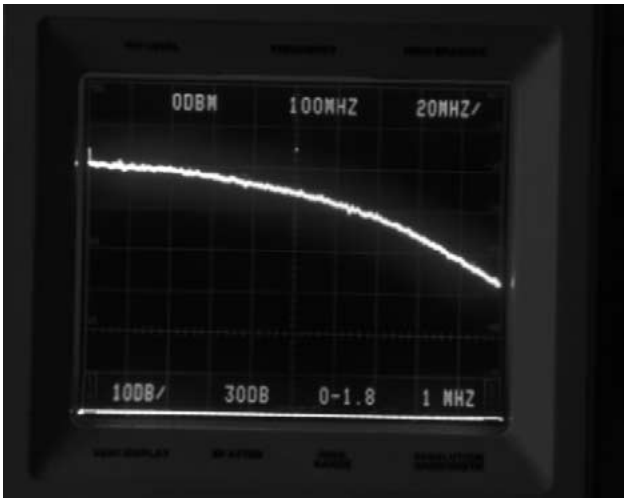

(a)

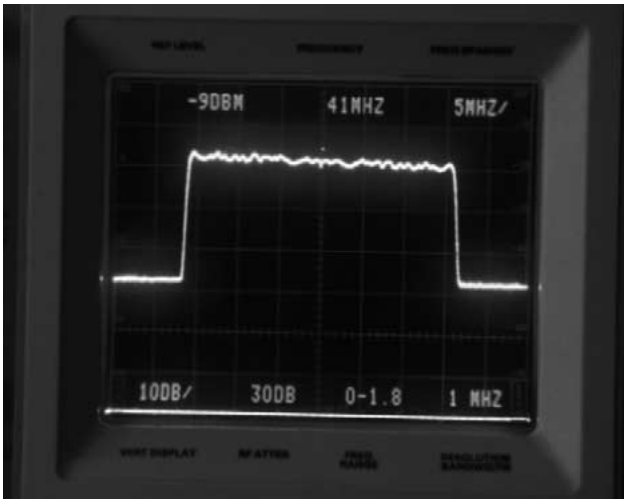

(a)

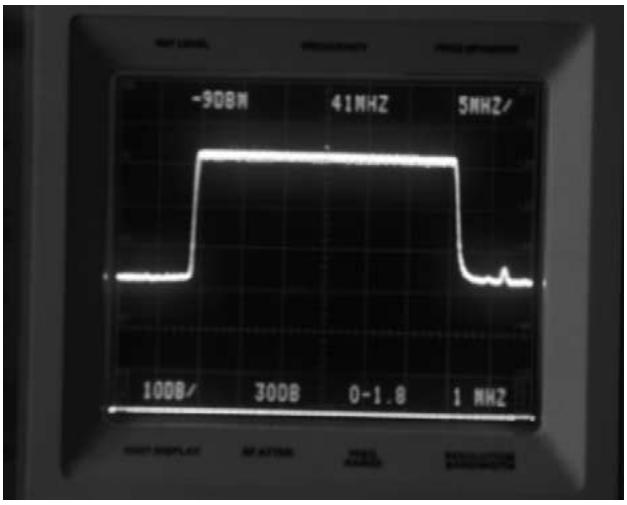

(c)

Fig. 2. Screen shots of spectrum analyzer showing noise power spectra produced by the AWG. (a) Full bandwidth, uncorrected spectrum resulting from independent, Gaussian distributed random numbers in each element of the AWG LUT. Note the roll-off of the spectrum above $\sim$ 100 MHz due to lowpass characteristics at the AWG output. (b) Spectrum band limited to 30 MHz and upconverted to 41 MHz by using $\sin c$ interpolation and sinusoidal modulation in software prior to loading into LUT (note expanded frequency scale). (c) Band-limited and upconverted signal with spectral prewhitening applied in software to remove hardware-induced coloration.

The uncorrelated noise components, $d_{A,B}$, are generated primarily by the active cold load termination in the modulator, followed by an isolator, directional coupler, and semirigid coaxial cabling. The brightness temperature of the active cold load is approximately equal to the noise temperature of the LNA which, in our case, is approximately 67 K. Combining that with the contribution from the passive devices that follow it results in a net brightness temperature of approximately 120 K. The brightness temperature of the correlated noise component, e, has been determined to be approximately 15 K. It is caused primarily by offsets between the ground reference of the analog noise signal being digitized and the zero voltage reference of the digitizer. A small fraction of the 15 K may also be due to leakage between the two AWG signal paths in the IF-to-RF modulator.

The brightness temperature of the AWG component of the signal $G_{A,B}c_{A,B}$ can be adjusted from 0 K to as high as 250 K before receiver saturation effects become significant. In practice, therefore, correlations in the signals x_A and x_B of anywhere between 4% and 69% can be achieved by adjusting the correlation of the AWG component between 0% and 100%.

In order to calibrate the raw measurements, it is necessary to correct for the offsets introduced by the CNCS hardware. To do this, correlation measurements are made with the AWG signal on and off. Turning the AWG off is equivalent to setting $c_{A,B} = 0$ in (21). The calibration algorithm for measurement of the cross correlation is, then

$$r_{AB} \equiv \frac{\langle x_{A,\mathrm{ON}} x_{B,\mathrm{ON}} \rangle - \langle x_{A,\mathrm{OFF}} x_{B,\mathrm{OFF}} \rangle}{\sqrt{(\langle x^2_{A,\mathrm{ON}} \rangle - \langle x^2_{A,\mathrm{OFF}} \rangle)(\langle x^2_{B,\mathrm{ON}} \rangle - \langle x^2_{B,\mathrm{OFF}} \rangle)}} \tag{22}$$

where the subscripts ON and OFF designate the state of the AWG. It is straightforward to show that $r_{AB} = \langle c_A c_B \rangle$. In addition to correcting for offsets in the correlation, by subtraction of the measurements in the OFF state, (22) also corrects for variations in the power levels of the individual signals, x and y. This is achieved by division by the geometric mean of the two self-correlations. This correction accounts for changes in the output power of the AWG, in the conversion loss of the upconverter, and in the insertion loss of all interconnecting transmission line. The accuracy of the corrections for both offset and power level is primarily limited by the switching time, between ON and OFF states in the case of the offset, and between cross- and self-correlations in the case of the power level. In practice, corrections accuracies of significantly better than 1.0 K can be achieved with moderate switching times of several seconds.

C. Demonstration of Radiometer Measurements

Two tests of the CNCS were conducted using the correlating receiver pair. In the first test, the magnitude of the complex correlation, ρ in (5), was held constant at 100% while its phase angle, θ in (5), was varied. Both receivers were operated at an ambient room temperature of $\sim$ 25 °C. Only the real part of the correlation was measured by the receiver pair during this test. The dependence of the measurement on θ is shown in Fig. 3. The ideal dependence, namely variation as $\cos(\theta)$, is also shown for comparison. The agreement between theory and measurement is best near phase angles of 0°, 90°, and 180° and there is a small

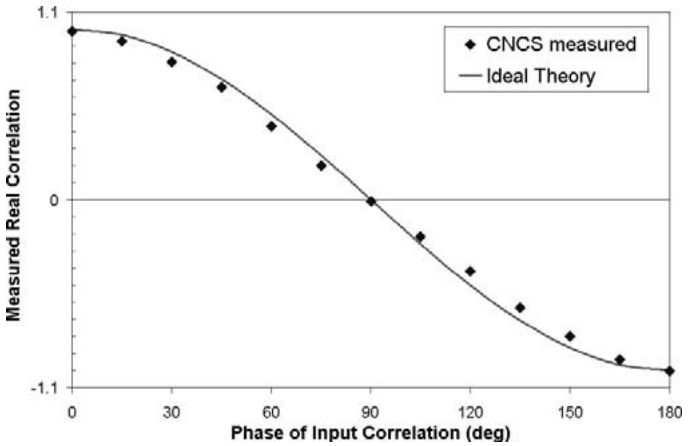

Fig. 3. Real part of complex cross correlation of a noise signal versus the phase of the correlation. In all case, the magnitude of the complex correlation is 100%.

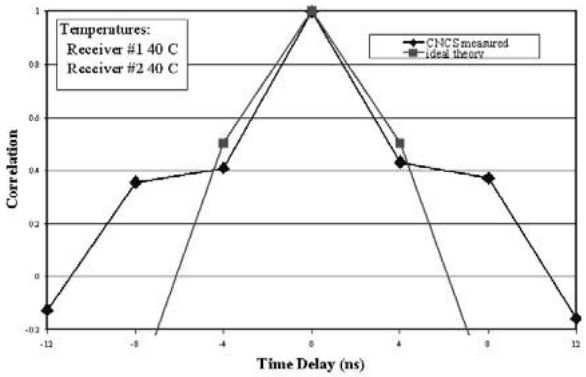

Fig. 4. Cross correlation of a common noise signal versus a time delay introduced into one of the signals by the CNCS. This is the fringe washing function for the receiver pair. Squares are the fringe washing predicted by theory for ideal boxcar receiver passband characteristics. Diamonds represent the measured fringe washing with both receivers operating at a physical temperature of 40 °C.

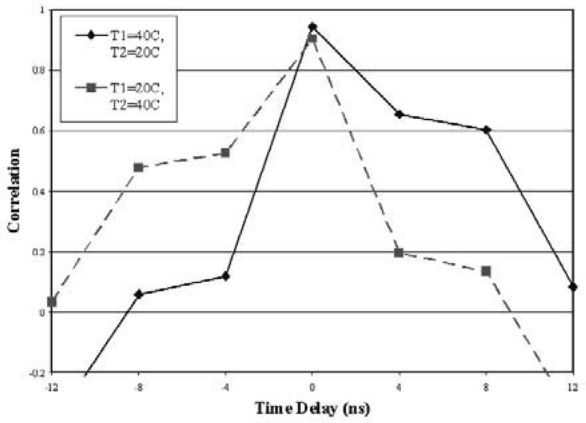

Fig. 5. Fringe washing function for the two cases. receiver #1 temperature = 40 °C and receiver #2 temperature = 20 °C (solid line + diamonds), and receiver #1 temperature = 20 °C and receiver #2 temperature = 40 °C (dashed line + squares). The maximum correlation at zero time delay has decreased relative to the case in Fig. 4 (of common temperatures) due to temperature-induced relative changes. Significant asymmetry has also been introduced into the fringe washing function at nonzero time delays.

but systematic discrepancy at intermediate angles. The probable cause of this behavior has been identified as an imbalance between the quantization thresholds of the two receivers' digitizers. At very high positive or negative correlations, the imbalance is effectively corrected by the offset correction described in (22). The imbalance has little effect when the two signals are uncorrelated. At intermediate levels of correlation, the imbalance introduces a systematic distortion into the results that is consistent with the observed behavior.

The sensitivity of the receivers to temperature imbalances was assessed in the second CNCS test. A variable time delay was added to one of the AWG signals in software, using the $\sin c$ interpolation method described above. The AWG signals were otherwise identical, i.e., the complex correlation had a magnitude of 100% and a phase angles of 0°. This variation in correlation with time delay is known as the "fringe washing function" for the receiver pair [25], [26]. The results are shown in Fig. 4 for the case of both receivers operating at a common physical temperature of 40 °C. Several characteristics of the receiver pair are revealed by its fringe washing function. Its maximum value, at zero time delay, indicates how well matched the two receivers are, just as in the first test. In this case, the maximum value of the fringe washing function is 99.9%. The variation of cross correlation with time delay is given by the autocorrelation of the signal, which is the Fourier transform of its noise power spectral density. In our case, the signal, $x(t)$, has a power spectrum roughly centered between 26 and 56 MHz. For an ideal flat spectrum with perfect phase matching across the passband, the autocorrelation is given by

$$r_{AB}(\tau) = \langle x(t)x(t-\tau)\rangle = B\frac{\sin(\pi B\tau)}{\pi B\tau}\cos(2\pi f_c\tau) \quad (23)$$

where $B = 30$ MHz is the bandwidth and $f_c = 41$ MHz is the center frequency of the power spectrum. The ideal fringe washing function given by (23) is also shown in Fig. 4 for comparison. The actual measurements roll off with time delay more slowly than is predicted by (23). This is likely a result of the nonideal passband shape of the actual receivers and of the differences between receivers in their phase and amplitude across the passbands.

Measurement of the fringe washing function was also performed with the receivers maintained at different physical temperatures inside independent environmental chambers. The results are shown in Fig. 5 for the cases of one receiver at 40 °C and the other at 20 °C and vice versa. In both cases, the maximum correlation, at zero time delay, has decreased significantly relative to the equal temperature case—to 90.4% and 94.4%. This could be due either to a decrease in the correlated gain of the receiver pair (due to temperature induced changes in their relative transfer functions), to a shift in the phase of the fringe washing function (due to temperature induced changes in the relative lengths of the interconnecting cables), or to some of both. The temperature difference has also introduced a significant asymmetry into the two fringe washing functions. (The fact that they are largely mirror reflections of one another when their temperatures are reversed indicates that the asymmetry is, indeed, due to the temperature difference.) Possible sources of the asymmetry include phase imbalances between the two receivers and the fact that samples of the fringe washing function are not symmetrically located on either side

of that time delay with maximum value. Additional measurements made with the CNCS have helped to isolate the probable cause of this fringe washing behavior as a temperature sensitive interconnecting stage within the receiver. An improved version of the receiver, with better tolerance of temperature changes, is currently in design.

VI. Summary and Discussion

A CNCS has been fabricated that is capable of producing pairs of stochastic noise signals with a wide range of individual and joint statistical properties. Individually, the bandwidth of the signals can be varied from significantly less than 1 MHz to more than 100 MHz. The upper and lower limits are set by the clock rate of the AWG and the record length of the LUT, respectively. In addition, the shape of the noise power spectra can be adjusted, with resolution limited also by the record length of the LUT. The total power in each individual signal can be varied between brightness temperatures of 120 K and greater than 350 K. The lower limit is set by the noise temperature of the active cold load in the CNCS upconversion modulator. The upper limit is set not by the CNCS itself but by the dynamic range of the radiometer under test. The magnitude of the partial correlation between the two signals can be varied between 4% and 69%. The lower limit is set by small correlated signals that are always present. They may be introduced by leakage and crosstalk in the CNCS itself or by bias characteristics of the correlating radiometers under test. The upper limit on the partial correlation is set by the RF losses present in the cabling between the CNCSs upconversion modulator and the radiometers. The complex phase angle of the partial correlation is adjustable independently of its magnitude. It can set to any value over the full range from 0° to 360°. In each of the above cases, the range of adjustability could be improved upon by using better hardware components.

The CNCS can be a useful tool for a variety of radiometer characterization studies. It can make rough measurements of the self-correlation gain and offset of an individual radiometer, but it cannot easily compete with the standard black body termination as a source of stable noise power. This is because the background power level of the CNCS active cold load, onto which any additional signal by the AWG is added, is generally not as steady as that of the thermal emission by a blackbody load with good temperature control. Cross correlation gain measurements can, on the other hand, be made with high precision and repeatability using the CNCS. This is principally because measurements of cross correlation are relative. They measure a percentage correlation between two signals and not their absolute strength. For example, the denominator in (22) normalizes the cross correlation with respect to the strengths of the individual signals. This normalization corrects for the gain of the two radiometers. It also corrects for any variation in the strength of the two CNCS signals. Thus, while the strength (and, hence, the self-correlation) of individual signals may vary somewhat, the normalization tends to remove the effects of that variation and keep the relative correlation coefficient much more stable.

There are some important aspects of correlating radiometer calibration that cannot be so readily addressed with the CNCS alone. In particular, antenna-related effects cannot be tested if the CNCS signals are injected via RF cabling directly into the input ports of the receiver. This is a case where the polarized load or some other controlled radiating source could provide valuable additional information about the instrument. Rather, it is in the laboratory during early system integration and testing of the radiometer, and after final antenna characterization as a means of convenient functional performance verification with Ground Support Equipment, that the CNCS should have the most value.

Acknowledgment

The authors wish to acknowledge the helpful suggestions by N. Skou (Danish Technical University) concerning design of the CNCS upconversion modulator.

References

[1] M. Born and E. Wolf, *Principles of Optics*. New York: Pergamon, 1975.
[2] G. E. P. Box and M. E. Müller, "A note on the generation of random normal deviates," *Ann. Math. Statist.*, vol. 29, pp. 610–611, 1958.
[3] W. N. Christiansen and J. A. Högbom, *Radiotelescopes*. Cambridge, U.K.: Cambridge Univ. Press, 1985.
[4] R. L. de Zafra, V. Chan, S. Crewell, C. Trimble, and J. M. Reeves, "Millimeter wave spectroscopic measurements over the south pole, III: The behavior of stratospheric nitric acid through the polar fall, winter, and spring," *J. Geophys. Res.*, vol. 102, pp. 1399–1410, 1997.
[5] D. T. Farley, "Incoherent scatter correlation function measurements," *Radio Sci.*, vol. 4, no. 10, pp. 935–953, 1969.
[6] M. Fischman and A. W. England, "Sensitivity of a 1.4 GHz direct-sampling digital radiometer," *IEEE Trans. Geosci. Remote Sensing*, vol. 37, pp. 2172–2180, Sept. 1999.
[7] A. J. Gasiewski and D. B. Kunkee, "Calibration and applications of polarization-correlating radiometers," *IEEE Trans. Microwave Theory Tech.*, vol. 41, pp. 767–773, May 1993.
[8] J. B. Hagen and D. T. Farley, "Digital-correlation techniques in radio science," *Radio Sci.*, vol. 8, no. 8, pp. 775–784, 1973.
[9] T. J. Jackson, D. M. Le Vine, C. T. Swift, T. J. Schmugge, and F. R. Schiebe, "Large area mapping of soil moisture using the ESTAR passive microwave radiometer in Washita-92," *Remote Sens. Environ.*, vol. 53, pp. 27–37, 1995.
[10] J. D. Kraus, *Radio Astronomy*. New York: McGraw-Hill, 1966.
[11] J. Lahtinen and M. Hallikainen, "Fully polarimetric calibration system for HUT polarimetric radiometer," in *Proc. IGARSS*, Honolulu, HI, 2000, pp. 1542–1544.
[12] D. M. Le Vine, M. Kao, R. Garvine, and T. Sanders, "Results from the Delaware coastal current experiment," *J. Atmos. Oceanic Technol.*, vol. 15, pp. 1478–1484, 1998.
[13] J. Li and C. S. Ruf, "Correlated noise calibration system for a multichannel interferometric radiometer," in *Proc. 1st Int. Microwave Radiometer Calibration Workshop*, Adelphi, MD, Oct. 30–31, 2000.
[14] M. Martin-Neira and Q. Garcia, "Pol-switching; Switching scheme for single channel polarimetric aperture synthesis radiometers," in *Proc. ESTEC*, 1999, Working Paper 2062, p. 23.
[15] P. J. Napier, A. R. Thompson, and R. D. Ethers, "The very large array: Design and performance of a modern synthesis radio telescope," *Proc. IEEE*, vol. 71, pp. 1295–1320, Nov. 1983.
[16] J. R. Piepmeier and A. J. Gasiewski, "Polarimetric scanning radiometer for airborne microwave imaging studies," in *Proc. IGARSS*, Lincoln, NE, 1996, pp. 1688–1691.
[17] A. Papoulis, *Probability, Random Variables, and Stochastic Processes*. New York: McGraw-Hill, 1984.
[18] C. L. Rino, "Radar measurements of ionosphere motion in the presence of current-induced spectral asymmetries," *Radio Sci.*, vol. 7, no. 11, pp. 1049–1060, 1972.
[19] C. S. Ruf, C. T. Swift, A. B. Tanner, and D. M. Le Vine, "Interferometric synthetic aperture microwave radiometry for the remote sensing of the earth," *IEEE Trans. Geosci. Remote Sensing*, vol. 26, pp. 597–611, Sept. 1988.
[20] C. S. Ruf and C. T. Swift, "Atmospheric profiling of water vapor density with a 20.5–23.5 GHz autocorrelation radiometer," *J. Atmos. Oceanic Technol.*, vol. 5, no. 4, pp. 539–546, 1988.

[21] C. S. Ruf, "Constraints on the polarization purity of a stokes microwave radiometer," *Radio Sci.*, vol. 33, no. 6, pp. 1617–1639, 1998.
[22] C. Ruf, C. Principe, T. Dod, B. Gosselin, B. Monosmith, S. Musko, S. Rogacki, A. Stewart, and Z. Zhang, "Lightweight rainfall radiometer STAR aircraft sensor," in *Proc. IGARSS*, vol. II, 2002, pp. 850–852.
[23] N. Skou and B. Laursen, "Measurement of ocean wind vector by an airborne, imaging polarimetric radiometer," *Radio Sci.*, vol. 33, no. 3, pp. 669–675, 1998.
[24] A. B. Tanner and C. T. Swift, "Calibration of a synthetic aperture radiometer," *IEEE Trans Geosci. Remote Sensing*, vol. 31, pp. 257–267, Jan. 1993.
[25] A. R. Thompson, J. M. Moran, and G. W. Swenson Jr., *Interferometry and Synthesis in Radio Astronomy*, 2nd ed. New York: Wiley, 2001, p. 672.
[26] F. Torres, A. Camps, J. Bara, and I. Corbella, "Impact of receiver errors on the radiometric accuracy of large two-dimensional aperture synthesis radiometers," *Radio Sci.*, vol. 32, no. 2, pp. 629–641, 1997.
[27] F. T. Ulaby, R. K. Moore, and A. K. Fung, *Microwave Remote Sensing Active and Passive*. Reading, MA: Addison-Wesley, 1981, vol. I, ch. 6, p. 456.
[28] S. Weinreb, "Digital radiometer," *Proc. IRE*, vol. 49, no. 6, p. 1099, 1961.
[29] F. J. Wentz, "Measurement of oceanic wind vector using satellite microwave radiometers," *IEEE Trans. Geosci. Remote Sensing*, vol. 30, pp. 960–972, Sept. 1992.
[30] S. H. Yueh, W. J. Wilson, S. V. Nghiem, F. K. Li, and W. B. Ricketts, "Polarimetric measurements of sea surface brightness temperature using an aircraft K-band radiometer," *IEEE Trans Geosci. Remote Sensing*, vol. 33, pp. 85–92, Jan. 1995.

Christopher S. Ruf (S'85–M'87–SM'92–F'01) received the B.A. degree in physics from Reed College, Portland, OR, and the Ph.D. degree in electrical and computer engineering from the University of Massachusetts, Amherst.

He is currently an Associate Professor of atmospheric, oceanic, and space sciences and electrical engineering and computer science at the University of Michigan, Ann Arbor. He has worked previously as a Production Engineer for Intel Corporation, Santa Clara, CA, as a member of the technical staff for the Jet Propulsion Laboratory, Pasadena, CA, and as a member of the faculty at Pennsylvania State University, University Park. During 2000, he was a Guest Professor at the Technical University of Denmark, Lyngby. His research interests include participation in the the current TOPEX/Poseidon, GEOSAT, Follow-On, and Jason-I, as well as SMOS, NPOESS, and TRMM/GPM flight missions, ground-based atmospheric remote sensing using millimeter radars and radiometers, and synthetic aperture radiometry. He is a past Associate Editor and Guest Editor for *Radio Science*.

Dr. Ruf is a member of the AGU, AMS, and URSI Commission F. He has received three NASA Certificates of Recognition and three NASA Group Achievement Awards, as well as the 1997 GRS-S Transactions Prize Paper Award and the 1999 IEEE Judith A. Resnik Technical Field Award. He is a past Editor of the IEEE GRS-S Newsletter and currently an Associate Editor of the IEEE TRANSACTIONS ON GEOSCIENCE AND REMOTE SENSING.

Jikang Li received the B.S. degree in atmospheric physics from Peking University, Beijing, China, in 1996, the M.S. degree in environmental engineering from the University of Cincinnati, Cincinnati, OH, in 1999, and the M.S. degree in electrical engineering from the University of Michigan, Ann Arbor, in 2002.

Her graduate research at the University of Cincinnati involved estimation of soil moisture profiles and surface fluxes by sequential assimilation of remotely sensed surface soil moisture. Her graduate research at the University of Michigan involved development of the correlated noise calibration standard and its application to microwave radiometer testing and characterization.